ELSEVIER

Journal of Petroleum Science and Engineering 19 (1998) 81–91

JOURNAL OF PETROLEUM SCIENCE & ENGINEERING

Application of composite membranes to determine relative permeabilities from displacement experiments

Hans M. Helset [a,*], Svein M. Skjæveland [b,1], George A. Virnovsky [a,2]

[a] *RF-Rogaland Research, P.O. Box 2503, N-4004 Stavanger, Norway*
[b] *Stavanger College, P.O. Box 2557, N-4004 Stavanger, Norway*

Abstract

Relative permeabilities are important characteristics of multiphase flow in porous media. Displacement experiments for relative permeabilities are usually interpreted by the JBN method neglecting capillary pressure. The experiments therefore have to be run at higher rates than those experienced during reservoir exploitation. Another disadvantage is that the relative permeabilities can only be determined for the usually small saturation interval outside the shock. We have developed a method to interpret displacement experiments with the capillary pressure included. The data needed are in situ measurements of saturations and phase pressures. The experiments can then be run at low flow rates, and relative permeabilities can be determined for all saturations. When using a short core, or if the saturation profile is spread out too much, the measurements can be affected by the end effect. We investigate using a combined water-wet and oil-wet membrane at the core outlet end to eliminate the end effect. With the membrane, the steady-state saturation profile is fairly uniform, and calculations of steady-state relative permeabilities are improved. However, because of the geometry of the membrane, the phases are separated at the core outlet. The separation results in increased flow resistance, and increased pressure in the core. Calculations of relative permeabilities for the traveling wave from pressure measurements after breakthrough will therefore be erroneous. © 1998 Elsevier Science B.V.

Keywords: membranes; end effect; core analysis; relative permeability; traveling wave

1. Introduction

Relative permeabilities are determined from flow experiments performed on core samples. The most direct way to measure the relative permeabilities is by the steady-state method. The two phases are simultaneously injected into the core at fixed rates until uniform saturation is obtained in the core. The saturation in the core is determined from material balance, or by weighing. In situ saturation measurements can also be used. The pressure drop over the core is also measured. Relative permeabilities at this saturation can then be determined directly from Darcy's law for each phase. Each measurement gives one point on the relative permeability curve (relative permeability vs. saturation). To determine the whole curve, the experiment has to be repeated at different

* Corresponding author. Fax: +47-5187-5200; e-mail: hans-martin.helset@rf.no
[1] Fax: +47-5183-1750; e-mail: s-skj@hsr.no
[2] Fax: +47-5187-5200; e-mail: george.virnovsky@rf.no

PII S0920-4105(97)00038-7

flow rate fractions. This method is therefore very time consuming.

Two-phase relative permeabilities can also be calculated from an unsteady-state (displacement) experiment. Typically, the core is initially saturated with one mobile fluid phase. This phase is then displaced by injecting the other phase into the core. Welge (1952) showed how to calculate the ratio of the relative permeabilities from a displacement experiment. Efros (1956) was the first to calculate individual relative permeabilities from displacement experiments. Later, Johnson et al. (1959) presented the calculation procedure in a more rigorous manner, and the method is therefore often called the JBN method. The unsteady-state method is often the preferred experimental method to determine the relative permeability relationship, both because it is much faster than the steady-state method, and because only one phase is injected.

The JBN method is based on the Buckley–Leverett theory of multiphase flow in porous media (Buckley and Leverett, 1942). The main assumption is to neglect capillary pressure. In homogeneous cores, capillary effects are most important at the outlet end of the core and over the saturation shock front. To suppress capillary effects, the experiment has to be performed at a high flow rate. Usually, these rates are higher than natural rates in reservoirs. Another major disadvantage is that relative permeabilities can only be calculated for the spreading part of the saturation profile. The theory is not valid in the vicinity of the saturation shock where capillary effects are significant. In a water–oil system with typical viscosities, the saturation shock interval can be more than 50% of the total mobile saturation range. This means that relative permeabilities cannot be determined for a substantial range in saturation. Extrapolating the relative permeability curves into the saturation interval corresponding to the saturation shock can be very difficult.

When the flow rate in the experiment is decreased, the capillary effects become more important. This will lead to a spreading of the shock front. The front will translate with a fixed shape, and is denoted as a traveling wave, or a stabilized capillary zone (Marle, 1981). If the saturation is not changing too much with time at a given location in the core, it is possible to make in situ measurements of saturation and pressures as the traveling wave profile passes by. We have recently developed a method to calculate relative permeabilities for the traveling wave part of the profile (Helset et al., 1996). A displacement experiment is performed at low rate such that the shock front is spread out into a traveling wave. In situ measurements of saturation and phase pressures are used to calculate relative permeabilities for a substantially larger saturation range than is possible with the standard JBN method. Calculation of relative permeabilities from the stabilized capillary zone has also been performed previously, but using only an approximate analysis (Kolltveit et al., 1990).

In situ saturation measurements can be performed by various techniques: X-ray attenuation (Oak et al., 1990), X-ray computer tomograph (CT) system (Hove et al., 1987), gamma emission (Kolltveit et al., 1990), ultrasound (Kalaydjian, 1992), microwaves (Honarpour et al., 1995) and NMR (Chen et al., 1993). In situ pressure measurements have been performed by several experimenters (Kolltveit et al., 1990; Kalaydjian, 1992; Honarpour et al., 1995).

When using a short core, or if the saturation profile is spread out too much, the measurements can be affected by the end effect, leading to errors in the calculated relative permeabilities. In this paper, we investigate using a combined water-wet and oil-wet membrane at the outlet end of the core to suppress the end effect. Previously, the effect of using a combined membrane at the inlet end has been studied (Virnovsky et al., 1995).

Because of the combined membrane at the core outlet, the phases are produced at separate exits. The capillary pressure, i.e. the difference in pressure between the water-outlets and the oil-outlets, can be set according to the saturation at the outlet end of the core. This might eliminate the end effect, and the core will act as a semi-infinite medium. To investigate the effects of the combined membrane, we perform 2D simulations of a core flood, both at unsteady-state and at steady-state conditions.

2. Equations

We now outline the derivation of the equations needed to calculate relative permeabilities for the

traveling wave part of the saturation profile. A complete treatment for three phases, and including gravity is given by Helset et al. (1996). Here we only consider two phase flow. In a displacement experiment the two phases are injected at fixed rate fractions into a core initially saturated with one or both phases. According to the Buckley–Leverett theory, the saturation profile will in general consist of a shock and a spreading part. When capillary effects are important, the shock will be spread out, and is called a traveling wave (Smoller, 1994). A traveling wave solution has the form (Virnovsky et al., 1994)

$$S(x, t) = S(\xi), \quad \xi = x - wt$$

Substituting $\xi = x - wt$, into the conservation equation

$$\frac{\partial u_1}{\partial x} + \phi \frac{\partial S_1}{\partial t} = 0 \tag{1}$$

and integrating gives

$$u_1 = C_1^* + \phi w S_1 = u(C_1 + v S_1) \tag{2}$$

where C_1^* is a constant of integration, $C_1 = C_1^*/u$ and $v = \phi w/u$. Inserting Eq. (2) into Darcy's law

$$u_1 = -\frac{k k_{r1}}{\mu_1} \frac{\partial p_1}{\partial x} \tag{3}$$

we obtain the pressure gradient along the traveling wave part of the saturation profile

$$\frac{\partial p_1}{\partial x} = -\frac{\mu_1}{k_{r1}} \frac{u}{k} (C_1 + v S_1) \tag{4}$$

Note that the expression for the pressure gradient only involves the relative permeability of one phase. The constant C_1 can be determined from $C_1 = f_1^+ - v S_1^+$, where $f_1^+ = f_1(S_1^+)$ and

$$f_1 = \frac{\lambda_1}{\lambda_1 + \lambda_2} \tag{5}$$

The velocity w of the traveling wave is the same as the velocity of the shock (Virnovsky et al., 1994)

$$w = \frac{u}{\phi} \frac{f_1^+ - f_1^-}{S_1^+ - S_1^-} \tag{6}$$

Here + and − denote the states in front of and behind the traveling wave, respectively. The velocity of the traveling wave can also be measured directly by monitoring the saturation profile at two different positions along the core.

Away from the traveling wave part of the profile, we can assume that the gradient of the capillary pressure can be neglected. The pressure gradient for this part is then the same for both phases (Collins, 1976)

$$\frac{\partial p_1}{\partial x} = \frac{\partial p_2}{\partial x} = -\frac{u}{k(\lambda_1 + \lambda_2)} \tag{7}$$

The pressure gradient at the traveling wave part of the saturation profile, Eq. (4), must necessarily follow the traveling wave. Using

$$\frac{\partial}{\partial x} p_1(x, t) = \frac{\partial}{\partial x} p_1(x - wt)$$

we get

$$\frac{\partial p_1}{\partial t} = \frac{\mu_1}{k_{r1}} \frac{wu}{k} (C_1 + v S_1) + w \frac{\partial}{\partial x} p_1(S_1^+) \tag{8}$$

where

$$\frac{\partial}{\partial x} p_1(S_1^+) = \text{const}$$

is the pressure gradient in phase 1 at the constant initial saturation S_1^+. Similar expressions can be derived for phase 2 (Helset et al., 1996).

Eq. (8) can be used to calculate the relative permeability of phase 1 from in situ measurements of saturation and phase pressure. First, a steady-state experiment is performed at the constant initial saturation S_1^+ to get $k_{r1}(S_1^+)$ and $k_{r2}(S_1^+)$. From Eq. (7) $(\partial/\partial x)p_1(S_1^+)$ is calculated.

If the saturation profile consists of only a traveling wave, the velocity w of the traveling wave is given from the initial and boundary conditions from Eq. (6). However, this is in general not known before the experiment is performed. To determine the velocity of the profile, the saturation must then be measured at two different locations along the core. Knowing the velocity w of the profile, the constant $C_1 = f_1(S_1^+) - w(\phi/u)S_1^+$ can be calculated. The time derivative $(\partial/\partial t)p_1(t)$ is calculated from the pressure measurements $p_1(t)$. Care has to

be taken when calculating the derivative of measured quantities. Alternatively, an integral method can be used as shown by Helset et al. (1996). The relative permeability $k_{r1}(S_1)$ can then be calculated from Eq. (8), which includes only known quantities.

In general, the saturation profile will consist of a combination of a traveling wave and a spreading wave. For a typical S-shaped fractional flow curve, the traveling wave will have higher velocity than the spreading part of the saturation profile. The expression in Eq. (8) is then still valid since it only involves quantities ahead of the traveling wave.

If the front of the traveling wave reaches the end of the core before the whole profile has passed the measurement point, the pressure gradient at the outlet end will also vary with time. Then Eq. (8) has to be modified as

$$\frac{\partial}{\partial t}p_1(x,t) = -w\frac{\partial}{\partial x}p_1(x,t) + w\frac{\partial}{\partial x}p_1(l,t) \tag{9}$$

with

$$\frac{\partial}{\partial x}p_1(l,t) = \frac{\partial}{\partial x}p_1(x,t-\Delta t)$$

and $\Delta t = (l-x)/w$

2.1. Length of the traveling wave profile

It is important to estimate the length of the stabilized zone. The profile must be wide enough so that measurements can be made, but the length should be small compared with the length of the core. For the traveling wave part of the saturation profile we have, following Marle (1981),

$$\frac{\partial S_1}{\partial x} = \frac{u}{k}\frac{\lambda_1+\lambda_2}{\lambda_1\lambda_2}\frac{1}{\mathrm{d}p_c/\mathrm{d}S_1}[C_1 + vS_1] \tag{10}$$

where we have neglected gravity for simplicity. By integrating Eq. (10), we get

$$X_D = \frac{k}{ul\mu_2}I \tag{11}$$

where X_D is the length of the traveling wave normalized with the length l of the core, and I is the integral

$$I = \int_{S_1^-}^{S_1^+}\frac{k_{r2}(\partial p_c/\partial S_1)}{(vS_1+C_1)(1+k_{r2}\mu_1/k_{r1}\mu_2)-1}\mathrm{d}S_1 \tag{12}$$

This is the same expression as given by Jones-Parra and Calhoun (1953), if we use

$$\frac{\partial f_1}{\partial S_1} = v$$

in the stabilized zone. The integration is taken over the whole saturation range of the traveling wave. However, the integrand is singular at the limits S_1^+ and S_1^-. The integration should therefore be performed over a slightly smaller saturation interval to avoid problems with the calculations.

If the saturation profile consists of both a spreading part and a traveling wave part, the saturation S_1^- in Eq. (11) will not be exactly the 'shock front saturation', but rather the saturation where the spreading part and the traveling wave part are connected (Le Fur, 1962).

The expression in Eq. (11) has also been used by Potter and Lyle (1994) to estimate the length of the stabilized zone. They only used qualitative estimates, and did not explicitly calculate the length of the zone.

3. Description of examples

We want to study the effects on the flow of having a composite membrane at the core outlet end.

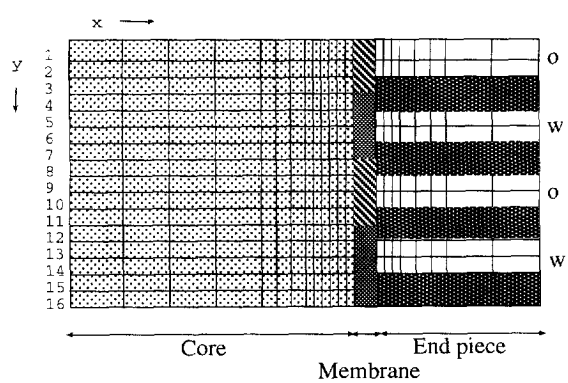

Fig. 1. Grid system used in the simulations, o = oil outlet, w = water outlet.

Table 1
Data for the simulation study

Length of the core	20 cm
Cross section area	10.64 cm^2
Core permeability k_h, k_v	133 md
ϕ	0.22
μ_1, μ_2	1.06, 1.30 cp
Residual saturations (S_{1r}, S_{2r})	0.20, 0.25
Thickness of membranes	0.015 cm
Membrane permeability	133 md
Initial saturation, S_1^+	0.75
Flow fraction at inlet, f_1^-	0.46
Total flow rate	1.0 cm^3/min
No. of grid blocks	133

To study spatial effects, we perform a 2D simulation of the core flood. The simplest membrane geometry would be that half of the membrane is water-wet and the other half is oil-wet. To decrease the effects of geometry we use the grid shown in Fig. 1. We have two water outlets and two oil outlets, separated by tight zones. In order to produce the phases separately, water-wet and oil-wet membranes are placed in front of the outlets. The membranes have equal permeability and thickness, and differ only in wettability. The threshold pressures for the membranes are high enough to ensure that there is no breakthrough of the other phase. The parameters used in the simulation are given in Table 1.

Realistic values of membrane permeability are 0.1 md–1 md. However, the small permeability of the membranes gives a significant pressure drop over the membrane, which can be accounted for. Here we want to study the flow inside the core. By using a membrane permeability of 133 md in the simulations, the pressure drop over the membrane is negligible.

The core is initially saturated with water and residual oil. Oil and water are simultaneously injected at constant rates. This is a secondary drainage process. We use a typical secondary drainage capillary pressure curve for Berea sandstone. For relative permeabilities we use Corey type functions with exponents $n_1 = n_2 = 2.0$, and end-point values $k_{r2}(S_{1r}) = k_{r1}(S_{2r}) = 1.0$.

To simplify the analysis, the fractional flow at the inlet is chosen such that the saturation profile consists of only a traveling wave. However, the conclusions arrived at here are also valid for the case when a spreading part is following the traveling wave. In this case two saturation measurements at different positions are needed to determine which part of the profile is moving as a traveling wave, and to determine the velocity.

The results from two different simulation runs are presented in the next section. All simulation parameters are equal in the two runs, while the boundary conditions at the outlet end of the core are different. In run 1 the difference in pressure between the oil exits and the water exits is set equal to the capillary pressure when no end effect is present. The outlet pressure is then varying with time as the profile passes the outlet. In run 2 the pressures at all exits are kept constant and equal.

4. Results

4.1. Saturation distribution

The saturation profiles from run 1 at different times are shown in Fig. 2. Row $y = 2$, is close to the oil outlet, while row $y = 6$ is close to the water outlet. The traveling wave saturation profile is translated with constant shape through the core, but is distorted at the membrane.

The spread of the saturation profile can be calculated from Eq. (11). Using the parameters from run 1 and taking the integration in Eq. (11) over the saturation range 0.46–0.74, we find that the length of the profile will be 3.3 cm. From the simulated saturation profiles, we find the length of the profile to be 4.8 cm. This means that there is some numerical dispersion in the simulations. We will not try to minimize this numerical dispersion, but rather use the same grid lengths and simulation parameters both for the short core (run 1 and 2) and for a long core used as a reference to illustrate a semi-infinite medium. This gives comparable results, even when numerical dispersion is present.

Comparing the profiles in Fig. 2 we see that the saturations close to the core outlet are non-uniform in the y-direction. The full saturation field close to the outlet at 25 min and 100 min is shown in Fig. 3. At 25 min, the traveling wave saturation profile is

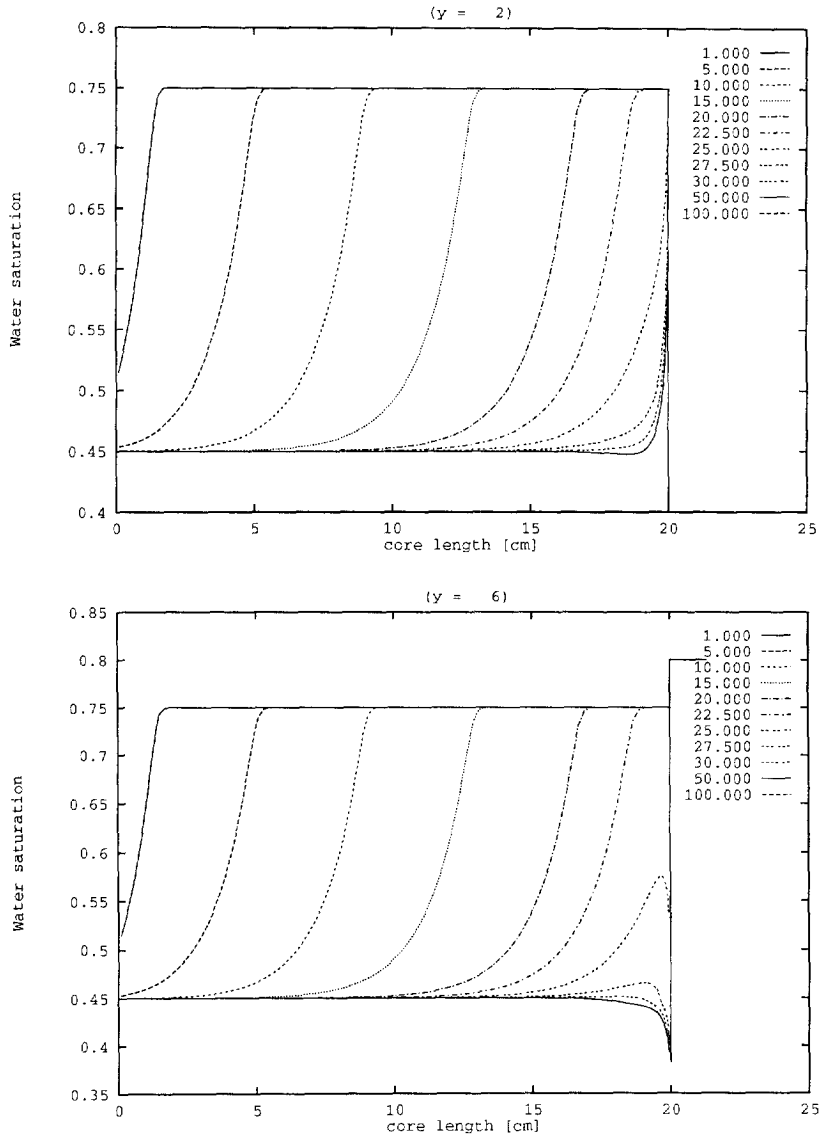

Fig. 2. Saturation profiles along row 2 (top) and row 6 (bottom) at different times for simulation run 1.

still passing the end of the core, while 100 min corresponds to steady state. Water saturation builds up at the oil outlets, while oil saturation is increased at the water outlets. Away from the end of the core, the saturation in the y-direction is uniform.

We average the saturation field from run 1 in the y-direction to compare the saturation profiles with predictions from 1D analysis. Fig. 4 shows the saturation averaged in the y-direction at times 25 min and 100 min (steady state) respectively. The average saturation is close to the 1D saturation profiles. The average saturations for run 1 and run 2 are almost identical at 25 min, while there is a significant difference at steady state. The end effect is almost eliminated at steady state when using the membranes. The best result was obtained in run 1.

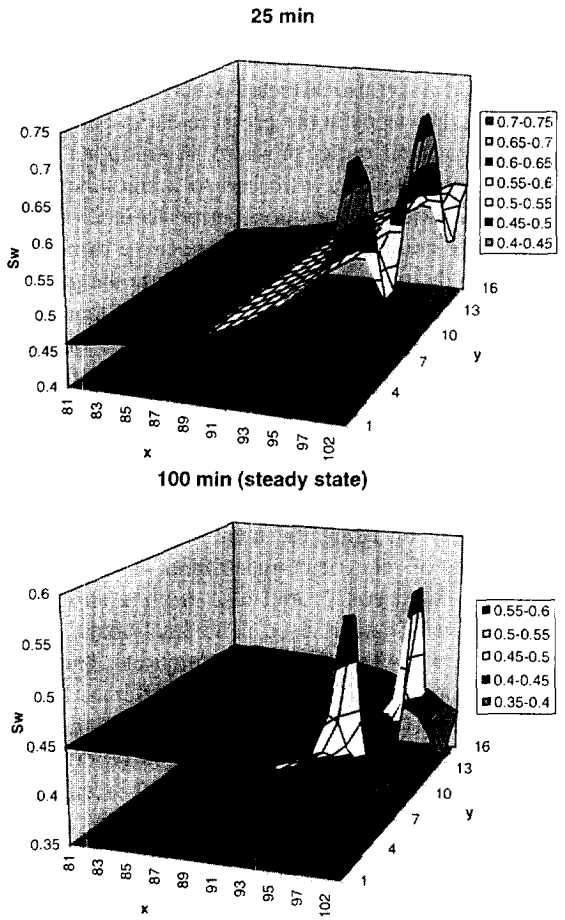

Fig. 3. Saturation field near the core outlet ($x = 16$–20 cm) at 25 min (top), and at 100 min corresponding to steady state (bottom).

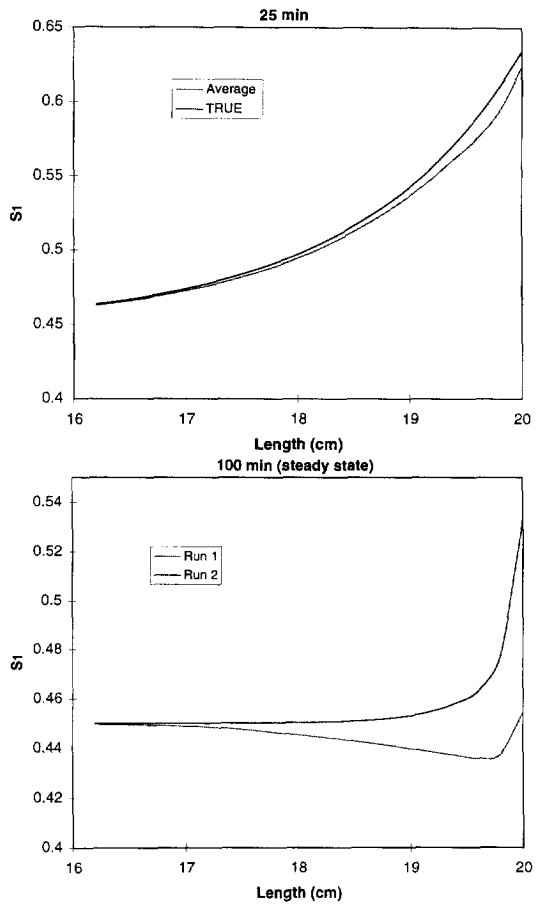

Fig. 4. Average saturations along the core. At times 25 min (top) the average saturation from run 1 is compared to the true saturation profile. At 100 min (steady state) the average saturations for run 1 and run 2 are shown.

4.2. Calculation of relative permeability

To calculate relative permeabilities for the traveling wave profile, we need in situ measurements of saturation and phase pressures. Usually, the measurements are taken in the middle of the core to avoid any end-effects. The saturation profile also needs a short time to stabilize after injection starts. The relative permeabilities are calculated from Eq. (8). Fig. 5 shows pressure vs. time from run 1 taken at $x = 10$ cm. Also shown is the theoretical pressure curve calculated from Eq. (8), and using the true relative permeability functions. The curves coincide quite well; the deviations are due to numerical dispersion in the simulation. This demonstrates that Eq.

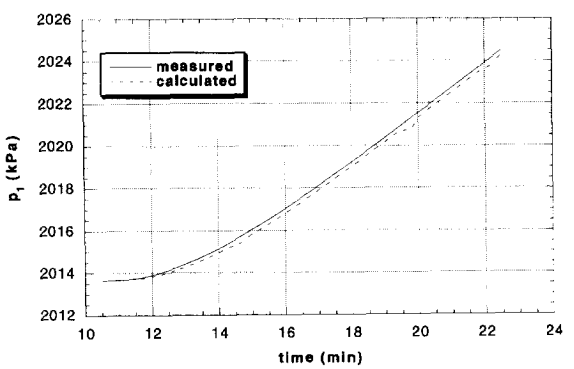

Fig. 5. Water pressure vs. time measured at $x = 10$ cm, i.e. at core half length. Also shown is the pressure curve calculated from Eq. (8).

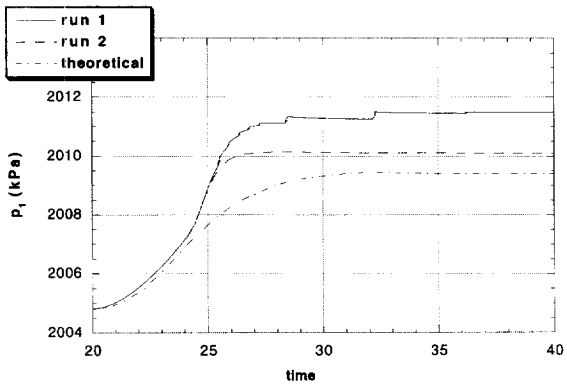

Fig. 6. Water pressure vs. time for run 1 and run 2 measured at $x = 17$ cm, i.e. 3 cm from the outlet end of the core. Also shown is the pressure curve calculated from Eq. (9).

(8) can be used to calculate the relative permeabilities for the traveling wave part of the saturation profile. More examples including calculation of relative permeabilities are given by Helset et al. (1996).

In a short core, or when the profile has a large spread, the front of the profile may reach the end of the core before the whole profile has passed the measurement point. Fig. 6 shows the water pressure vs. time measured at $x = 17$ cm, i.e. 3 cm from the core outlet. This illustrates using a 6 cm core and taking measurements at core half-length. Results from run 1 and run 2 are shown. The theoretical curve calculated using Eq. (9) is shown for comparison. When calculating relative permeabilities, the gradient $\mathrm{d}p_i/\mathrm{d}t$ is used. Before approximately 24 min, corresponding to the breakthrough time for the traveling wave, all three curves have the same gradient. After 24 min, both simulated curves deviate from the theoretical curve. When the front reaches the end of the core, oil and water have to redistribute in order to be produced at different exits. There is a significant pressure rise due to this redistribution of fluids, and the gradient is a factor 3 too large, leading of course to large errors in the calculated relative permeabilities.

There is also a difference between the pressure curves from run 1 and run 2. In run 1 the pressure difference between the oil outlets and the water outlets is set equal to the capillary pressure corresponding to the saturation at the outlet. The pressure at the water outlet is kept constant, while the oil outlet pressure is varying with time. In run 2 all outlet pressures are equal and constant. Water pressure in run 1 is also affected when oil pressure is increased. The steps in the pressure curve correspond to changes in oil outlet pressure. A smoother variation in outlet pressure will lead to a smoother pressure curve. After a transition period from 24 min to 27 min, the gradient of the pressure curve from run 1 is close to the theoretical gradient, while the gradient from run 2 differs significantly from the theoretical gradient. The same effects are seen in the oil pressure curve, also having an extra pressure increase in the period where the fluids are rearranging. Using data from this transition period will give errors in calculations of relative permeabilities.

From Fig. 4 we see that the end effect is almost eliminated when using the membrane. We compare calculations of relative permeabilities at steady state from run 1 and run 2, and also from a simulation when no membrane is used. The fractional flow of water is $f_1 = 0.45$ in all three simulations. The average saturation in the y-direction is different for the different outlet boundary conditions, and the total average saturation in the core will also be different. The relative permeabilities calculated at steady state are shown in Fig. 7, together with the true relative permeability curve. Reducing the core length will increase the influence of the end effect on the average saturation in the core.

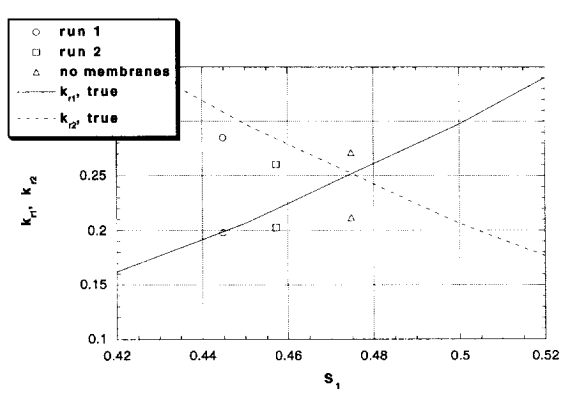

Fig. 7. Calculations of relative permeabilities at steady state with different outlet boundary conditions, compared to the true relative permeability curves.

5. Discussion

A method to calculate relative permeabilities from the traveling wave part of the saturation profile has been presented. In situ measurements of saturations and phase pressures are needed. To be able to make good measurements of saturation and pressure over the traveling wave part of the saturation profile, the traveling wave must be sufficiently spread out. This can be controlled by lowering the injection rate. The spread of the profile can be estimated from Eq. (11), or from simulation. In either case, an initial guess of relative permeabilities and capillary pressure is needed, giving only a rough estimate of the true saturation profile.

When capillary effects are strong, or when using short cores, the front of the traveling wave will reach the end of the core before the whole traveling wave has passed the measurement point. Because of the end effect, saturation and pressure profiles will be disturbed, and measurements taken after breakthrough cannot be interpreted. It is also seen from simulation that it takes a finite (however small) time for the traveling wave to stabilize, depending on the ratio of viscous to capillary forces. Measurements should therefore not be taken too close to the core inlet.

In order to minimize the end effect, the use of a combined water-wet and oil-wet membrane at the outlet was studied by simulation. The membrane allows both phases to flow out of the core, and there are only minor accumulations of the phases. Best results were obtained when using a pressure difference between the water and oil outlets corresponding to the capillary pressure inside the core.

The geometry of the outlet endpiece plays an important role, as can be seen from figures of the saturation field close to the outlet end of the core. Water is accumulated at the oil exits, while oil accumulates at the water exits. From having a uniform saturation distribution in a core cross section in the center part of the core, the phases are separated when the saturation front reaches the end of the core. The saturation averaged in the y-direction is relatively close to the saturation profile from 1D calculations, both at transient and steady-state conditions.

However, the pressure vs. time data show an extra increase in phase pressures due to the separation of the phases at the outlet. The effect of the separation can be minimized by constructing the membrane of several regions that are alternately water-wet and oil-wet. However, it might be difficult to completely eliminate the effect of phase separation at the outlet. Increased understanding of the separation process close to the core outlet is therefore needed. However, to model the separation, and thereby fully account for the extra pressure buildup might be very difficult. This means that only measurements performed before breakthrough can be interpreted properly to calculate relative permeabilities for the traveling wave. The measurements of phase pressures should therefore be ended when the tip of the traveling wave reaches the end of the core. The membrane will in this case only serve to suppress the extent of the end effect.

6. Conclusion

A method for calculating relative permeabilities from the traveling wave part of the saturation profile in a displacement experiment has been derived. In the analysis, capillary pressures are included. From this analysis, relative permeabilities from displacement experiments can be determined for the whole saturation range, in contrast to the traditional JBN method which is not valid at the saturation shock. Using the new method, it is also possible to perform the experiments at low flow rates corresponding to realistic reservoir rates. The experimental data needed are in situ measurements of saturation and phase pressure. The equations for determining the relative permeabilities for each phase are decoupled, meaning that the determination of relative permeability of one phase only depends upon the saturation and pressure of that phase.

The traveling wave profile can be distorted by an end-effect. The consequences of using a combined water-wet and oil-wet membrane at the core outlet end to suppress the end-effect have been studied by 2D simulation. The main conclusions are:

- The combined membrane allows both phases to flow out of the core.
- The saturation distribution is non-uniform close to the membrane. Water accumulates at the oil outlets, and oil accumulates at the water outlets.

· The average saturation in a cross section of the core is close to the saturation from 1D calculations. At steady state the average saturation deviates only 1–2% from a uniform saturation throughout the core.

· Using a pressure difference between the water and oil outlets corresponding to the capillary pressure inside the core reduces the end effect more than having all outlet pressures equal.

· The phases are separated close to the core outlet to flow through different regions of the membrane. The separation of phases leads to increased flow resistance and increased pressure in the core. Only in situ pressure measurements taken before breakthrough can be interpreted to calculate relative permeabilities for the traveling wave.

7. Nomenclature

C	constant of integration (dimensionless)
f	fractional flow (dimensionless)
k	permeability, L^2 (m^2)
l	length of the core, L (m)
p	pressure, m/Lt^2 (Pa)
S	saturation (dimensionless)
t	time, t (s)
u	Darcy velocity, L/t (m/s)
v	$w\phi/u$ (dimensionless)
w	velocity of traveling wave, L/t (m/s)
x, y	spatial coordinates, L (m)
X	length of traveling wave, L (m)
λ	mobility, L^3t/m (m^2/Pa · s)
μ	fluid viscosity, m/Lt (Pa · s)
ϕ	porosity
ξ	traveling wave coordinate, L (m)

Subscripts

c	capillary
D	dimensionless
h	horizontal
i	fluid phase; $i = 1,2$
r	relative, residual
v	vertical

Superscripts

+	right state of a shock
−	left state of a shock

References

Buckley, S.E., Leverett, M.C., 1942. Mechanism of fluid displacement in sands. Trans. AIME 146, 107.

Chen, S., Qin, F., Kim, K.-H., Watson, A.T., 1993. NMR imaging of multiphase flow in porous media. AIChE J. 39 (6), 1473–1479.

Collins, R.A., 1976. Flow of Fluids through Porous Materials. PennWell, Tulsa, OK.

Efros, D.A., 1956. Determination of relative permeabilities and distribution functions at water–oil displacement. Dokl. Akad. Nauk 110 (5), 746–749, in Russian.

Helset, H.M., Nordtvedt, J.-E., Skjæveland, S.M., Virnovsky, G.A., 1996. Three-phase relative permeabilities from displacement experiments with full account for capillary pressure. Paper SPE 36684, to be presented at the Annual Technical Conf. and Exhibition held in Denver, CO, USA, 6–9 October.

Honarpour, M.M., Huang, D.D., Dogru, A.H., 1995. Simultaneous measurements of relative permeability, capillary pressure, and electrical resistivity with microwave system for saturation monitoring. Paper SPE 30540 presented at the SPE Annual Technical Conf. and Exhibition held in Dallas, USA, 22–25 October.

Hove, A., Ringen, J.K., Read, P.A., 1987. Visualization of laboratory corefloods with the aid of computerized tomography of X-rays. SPE Res. Eng., May, 148.

Johnson, E.F., Bossler, D.P., Naumann, V.O., 1959. Calculation of relative permeability from displacement experiments. Trans. AIME 216, 370.

Jones-Parra, J., Calhoun, J.C. Jr., 1953. Computation of a linear flood by the stabilized zone method. Trans. AIME 198, 335–338.

Kalaydjian, F.J.-M., 1992. Dynamic capillary pressure curve for water/oil displacement in porous media: theory vs. experiment. Paper SPE 24813 presented at the 67th Annual Technical Conf. and Exhibition of the SPE, Washington, DC, October 4–7.

Kolltveit, K., Nordtvedt, J.-E., Hovland, F., Kvanvik, B.A., Lie, B., 1990. Using explicit and implicit methods to calculate relative permeabilities from in situ measurements. Paper presented at the 1st Society of Core Analysts European Core Analysis Symp., London, UK, 21–23 May.

Le Fur, B., 1962. Influence de la capillarite et de la gravite sur le deplacement non miscible unidimensionnel dans un milieu poreux. J. Mecanique 1 (2), 213.

Marle, C.M., 1981. Multiphase Flow in Porous Media. Editions Technip, Paris.

Oak, M.J., Baker, L.E., Thomas, D.C., 1990. Three-phase relative permeability of Berea sandstone. J. Pet. Tech. 42, 1054–1061.

Potter, G., Lyle, G., 1994. Measuring unsteady-state gas displacing liquid relative permeability of high permeability samples. Paper SCA-9419 presented at the 1994 Int. Symp. of the Society of Core Analysts, Stavanger, Norway, September 12–14, pp. 207–216.

Smoller, J.. 1994. Shock Waves and Reaction-diffusion Equations. 2nd ed. Springer, New York.

Virnovsky, G.A., Helset, H.M., Skjæveland, S.M., 1994. Stability of displacement fronts in WAG operations. Paper SPE 28622 presented at the SPE 69th Annual Technical Conf. and Exhibition in New Orleans, LA, USA, September 25–28.

Virnovsky, G.A., Guo, Y., Skjæveland, S.M., 1995. Relative permeability and capillary pressure concurrently determined from steady-state flow experiments. Paper presented at the European IOR Symp. in Vienna, Austria, May 15–17.

Welge, H., 1952. A simplified method for computing oil recovery by gas or water drive. Trans. AIME 195, 91.